Size-Selective Catalytic Growth of Nearly 100% Pure Carbon Nanocoils with Copper Nanoparticles Produced by Atomic Layer Deposition

Guizhen Wang,[†,‡,⊥] Gu Ran,[§,⊥] Gengping Wan,[‡] Peng Yang,[†] Zhe Gao,[†] Shiwei Lin,[‡] Chuan Fu,[§,*] and Yong Qin[†,*]

[†]State Key Laboratory of Coal Conversion, Institute of Coal Chemistry, Chinese Academy of Sciences, Taiyuan, 030001, People's Republic of China, [‡]Key Laboratory of Chinese Education Ministry for Tropical Biological Resources, Hainan University, Haikou, 570228, People's Republic of China, and [§]School of Chemistry and Environmental Engineering, Chongqing Three Gorges University, Chongqing, 404100, People's Republic of China. [⊥]G.W. and G.R contributed equally to this work.

ABSTRACT In this paper, Cu nanoparticles with narrow size distribution are synthesized by reduction of CuO films produced by atomic layer deposition (ALD), which are used as catalysts for the catalytic growth of carbon nanostructures. By properly adjusting the ALD cycle numbers, the size of produced Cu nanoparticles can be well controlled. Uniform carbon nanocoils with near 100% purity can be obtained by using 50−80 nm Cu nanoparticles, while thin straight fibers and thick straight fibers are produced by applying 5−35 and 100−200 nm Cu nanoparticles, respectively. The mechanism of the particle size-dependent growth of the carbon nanostructure was analyzed based on the experimental results and theoretical simulation. Our results can provide important information for the preparation of helical carbon nanostructures with high purity. Moreover, this work also demonstrates that ALD is a viable technique for synthesizing nanoparticles with highly controllable size and narrow size distribution suitable for studying particle size-dependent catalytic behavior and other applications.

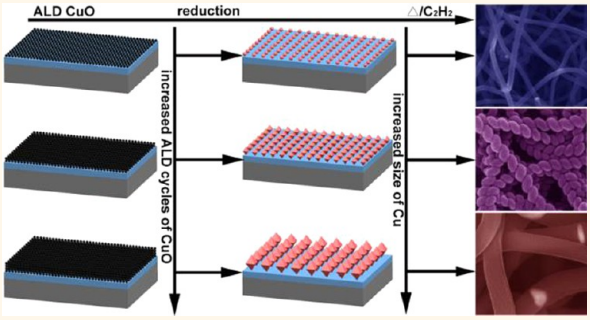

KEYWORDS: atomic layer deposition · carbon nanocoils · high purity · Cu nanoparticles · size-selective catalytic

As one of the most technologically important types of carbon nanomaterials, carbon nanocoils (CNCs) possess unique geometrical elegance and are attracting increased interest as a result of their unique mechanical, thermal, electric, and magnetic properties.[1−6] Potential applications for such novel carbon species span structural foams for cushioning and energy dissipation,[7] microwave absorbers in stealthy coating,[8,9] and field emission properties in flat-panel displays.[10,11] Usually, the performances and potential applications of CNCs are bound up with their morphology and geometry. For instance, the CNCs are representative chiral materials and exhibit wavelength selectivity when used as electromagnetic wave absorbers due to their chiral parameters determined by the coil pitch and diameter.[12,13] Pan *et al.* researched the field emission properties of CNCs and found that the turn-on voltage decreased by decreasing the coil diameter.[14] Therefore, developing a simple method with good selectivity and repeatability to synthesize highly pure CNCs with uniform coil pitch and diameter would be most desirable from both fundamental and practical points of view.

Generally, CNCs are prepared by chemical vapor deposition (CVD) employing metal nanoparticles as catalysts.[3,5,15−17] Many researchers have performed detailed experiments to investigate the effects of synthesis parameters on the selectivity of CNCs. Growth temperature,[18] atmosphere,[19] particle size of catalyst,[20,21] and the composition of catalysts[3,22−24] were found to be several key factors in the formation of helical structures. Among them, the particle size of the

* Address correspondence to casual2005@163.com, qinyong@sxicc.ac.cn.

Received for review March 28, 2014 and accepted May 1, 2014.

Published online May 01, 2014
10.1021/nn501709h

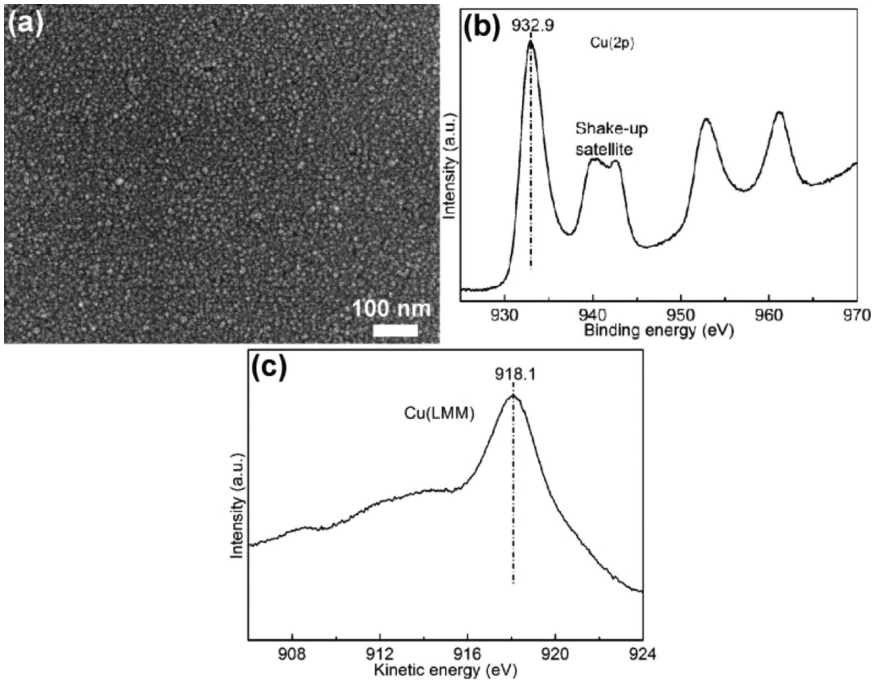

Figure 1. (a) SEM image of CuO films by applying 400 ALD cycles. High-resolution XPS spectra of the (b) Cu(2p) and (c) Cu(LMM) regions.

catalyst may substantially conduct the growth of CNCs. A small size of catalyst particles usually favors formation of helical fibers, while large size of catalysts results in straight fibers. Other factors, such as atmosphere, temperature, and the composition of catalysts also affected output of the helical structures by influencing the particle size of the catalyst. However, limited to the technological hurdles of traditional methods including the size and size distribution control of the catalytic particles, it is still a great challenge to synthesize CNCs with uniform morphology and high purity.

Atomic layer deposition (ALD) is a versatile coating technique that produces films with uniform and conformal thickness by a sequence of self-limiting reactions of gas-phase precursor molecules.[25−27] However, when the ALD chemistry is inhibited on the starting substrate or when the ALD material aggregates from surface diffusion, ALD is a promising method for the production of nanoparticles and has been used recently to synthesize supported noble metal nanocatalysts exhibiting remarkably high activity.[28−31] Herein, we present a simple, controllable, and reproducible strategy for the growth of nearly 100% pure CNCs. Highly dispersed Cu nanoparticles with size-dependent catalytic characteristics have been produced by *in situ* reduction of CuO deposited by ALD, which can decompose acetylene to effectively produce uniform CNCs. We also studied the effect of particle size on selective CNC growth and performed detailed investigations and theoretical simulations to elucidate the size-dependent growth mechanism.

RESULTS AND DISCUSSION

The surface morphology of CuO thin films was first examined by scanning electron microscopy (SEM). A typical surface morphology of CuO films from 400 ALD cycles is characterized by dense, tiny, granular crystallites (Figure 1a). SEM images of other samples prepared with various ALD cycles are provided in Figure S1 (see Supporting Information), all of which reveal the similar granulometric morphology. XPS analysis was performed to determine the composition of the CuO layer. Figure 1b and c show the XPS spectra of CuO/Al_2O_3-(5 nm)/Si substrate obtained by applying 50 ALD cycles of Al_2O_3 and then 400 cycles of CuO deposition. The peak positions of Cu(2p) and Cu(LMM) (LMM: transition between inner shells L and M) and the shakeup satellite features on the higher binding energy side of the Cu(2p) main peak clearly demonstrate that the dominant component of the product is CuO.[32] The strong oxidation ability of O_3 in the present system precludes the mixing of incompletely oxidized forms of Cu and Cu_2O and induces higher oxidation states.

The CuO films can be converted into Cu nanoparticles with narrow size distribution by reduction with hydrogen (5% H_2/N_2 atmosphere) (Figure 2). The particle size of Cu nanoparticles clearly increases with the increase of ALD cycles of CuO. However, in this work, the CuO nanoparticle films are directly used as catalysts for the growth of CNCs without the hydrogen reduction step because acetylene undergoes slight decomposition at high temperature, leading to the release of reducing hydrogen.[33] Low-magnification FE-SEM image (Figure 3a) reveals that CNCs with a

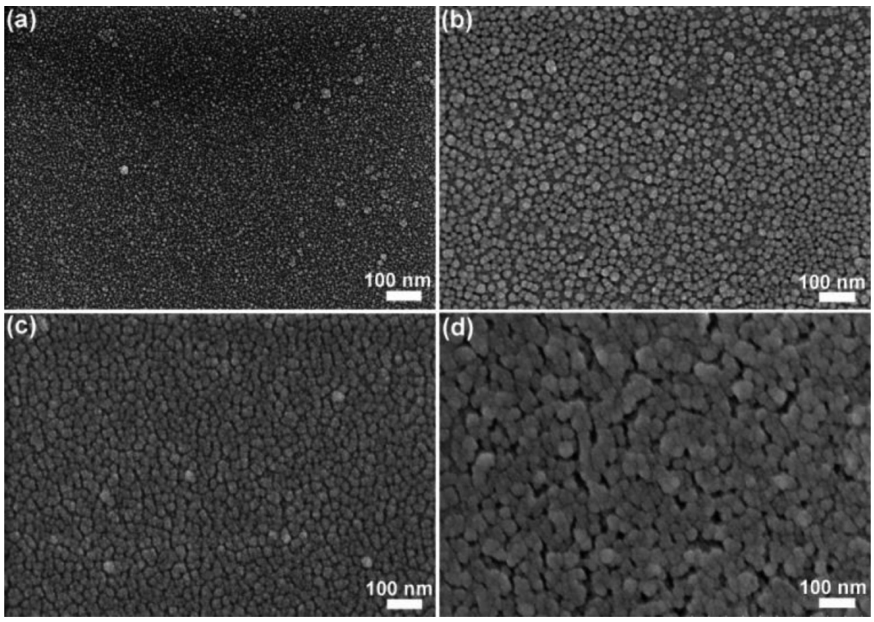

Figure 2. SEM images of Cu nanoparticles obtained by applying (a) 200, (b) 400, (c) 800, and (d) 1200 ALD cycles of CuO deposition, respectively, and then a reduction process in 5% H_2/N_2 atmosphere.

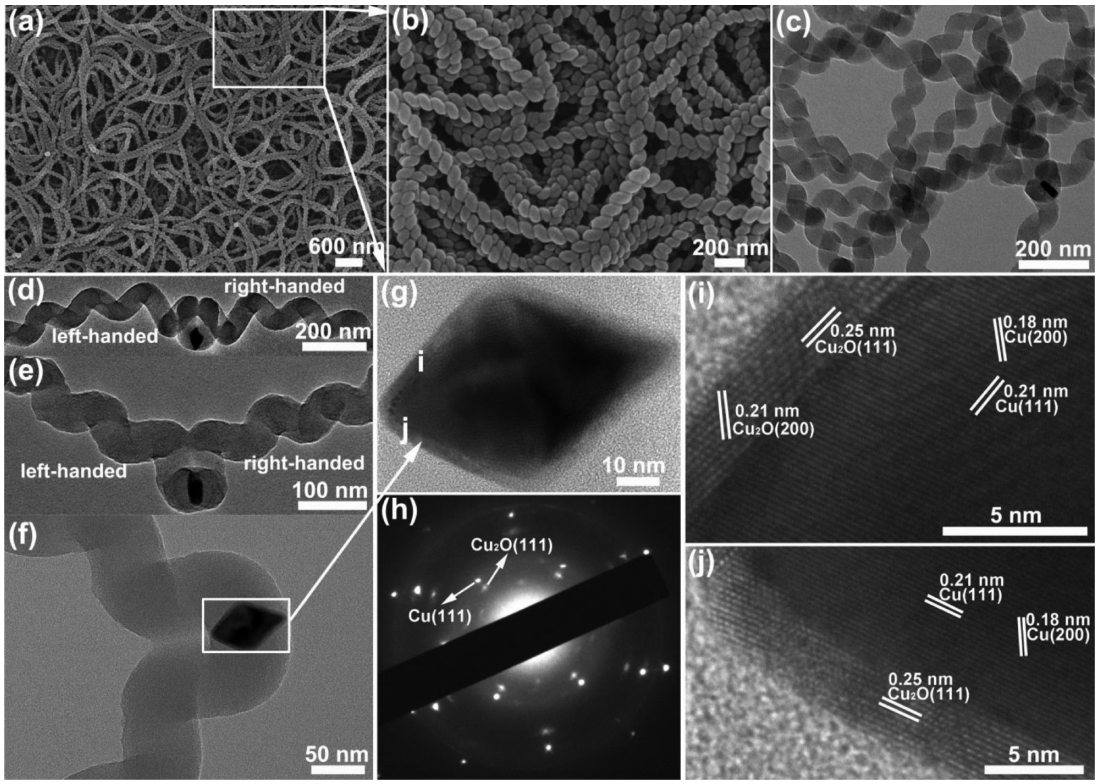

Figure 3. Typical (a, b) SEM and (c–f) TEM images of as-synthesized CNCs. (g) TEM, (h) SEAD, and (i, j) HRTEM images of an individual catalyst particle from CNC in (f).

quite high purity were obtained by the thermal decomposition of acetylene at 260 °C by using 400 ALD cycles of CuO as catalyst (precursor). In this sample, there is almost no straight fiber from SEM images by observing multiple random areas, suggesting the present CuO films prepared by ALD are extraordinarily effective for the growth of highly pure, regularly coiled carbon nanofibers. Most important of all, such highly pure CNCs can be reproducibly produced in a wide CuO deposition range of 350–450 ALD cycles (Figure S2). The high-magnification SEM image shown in Figure 3b demonstrates that all these fibers are in the form of single

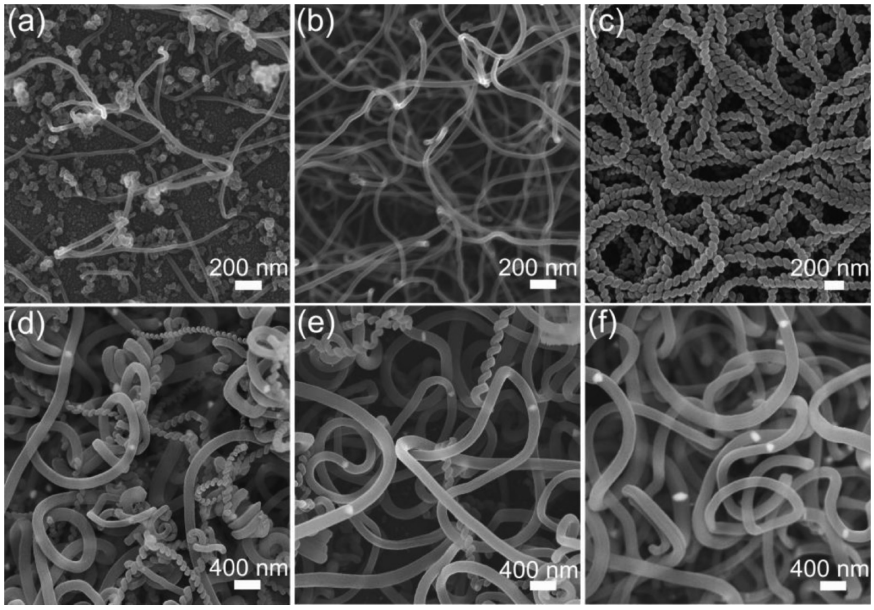

Figure 4. SEM images of the products obtained with (a) 100, (b) 200, (c) 400, (d) 600, (e) 800, and (f) 1200 ALD cycles of CuO deposition.

coils. Coil diameters of the CNCs are estimated to be about 80−120 nm, and each fiber exhibits constant coil diameter and coil pitch, indicating that the fiber growth was stable and not sensitive to external influence in the whole growth process.

The morphology and structure of these CNCs are further investigated by transmission electron microscopy (TEM), as shown in Figure 3c. The helical morphology of nanofibers can be clearly seen, in good agreement with the SEM observation. These nanofibers always consist of two twin helices with opposite chiralities based on the catalyst particles located at the middle; namely, one is left-hand coiled and the other is right-hand coiled (Figure 3c and d). Furthermore, it can be seen that almost perfect symmetry is constructed between them in the helical structure including fiber diameter, cycle number, coil diameter, and coil pitch. The catalyst particles are about 50−80 nm in diameter and can be mainly divided into two categories of morphology, octahedron and triangular prism. An individual catalytic nanoparticle is observed from Figure 3f and g and characterized to be Cu with a small amount of O element by energy-dispersive X-ray spectroscopy (EDS) (Figure S3). Selected area electron diffraction (SAED) analysis (Figure 3h) confirms that it consists of metallic Cu and Cu_2O phases. The high-resolution TEM (HRTEM) image (Figure 3i and j) highlights the well-defined crystalline lattice spacing of 0.18 and 0.21 nm indexed as (100) and (111) crystal planes of Cu in the core and 0.21 and 0.25 nm for Cu_2O in the thin edge (shell), respectively. Because of the poor stability of nanoscaled Cu in air, the thin Cu_2O shell should be from the partial oxidation of Cu nanoparticles when exposed in air after carbon nanofiber growth.[34] The XRD pattern of CNCs shows that only diffraction peaks of amorphous carbon fibers and Cu can be found (Figure S4), further revealing that Cu is indeed the active component for the catalyzed growth of CNCs.

The effect of ALD cycle numbers of CuO on the fiber structures was investigated. Figure 4 shows the typical SEM images of the products grown on the substrate with 100, 200, 400, 600, 800, and 1200 ALD cycles of CuO deposition, respectively. Interestingly, with the increase of ALD cycles, the products clearly underwent a morphological evolution from thin straight fiber (TNF) to helical fiber to thick straight fiber (TKF). At first, when 100 ALD cycles of CuO were applied, a small number of TNFs with a diameter of about 10−25 nm were produced (Figure 4a). Typically, for 200 ALD cycles of CuO, a high yield of TNFs with a uniform linear structure was obtained as shown in Figure 4b. The TNFs have an increased diameter of about 20−35 nm. As mentioned above, highly pure helical fibers can be obtained with 400 ALD cycles of CuO (Figure 4c). When the cycle number was further increased from 600 to 1200 ALD cycles, the products present an obvious transition from helical to linear structure (Figure 4d−f). The diameter of the TKFs is about 100−200 nm and also relatively uniform for 1200 ALD cycles of CuO (Figure 4f), similar to the results reported previously.[19]

Further SEM and TEM characterization were performed to determine the detailed structure of the two kinds of straight fibers. For TNFs, it should be noticed that all of these catalyst particles are nearly spherical in shape located at one end of the fibers, as shown in Figure 5a. General statistics from TEM observations (Figure 5b−d and Figure S5) reveal that the catalysts with a size of 5−35 nm grow TNFs with a fiber

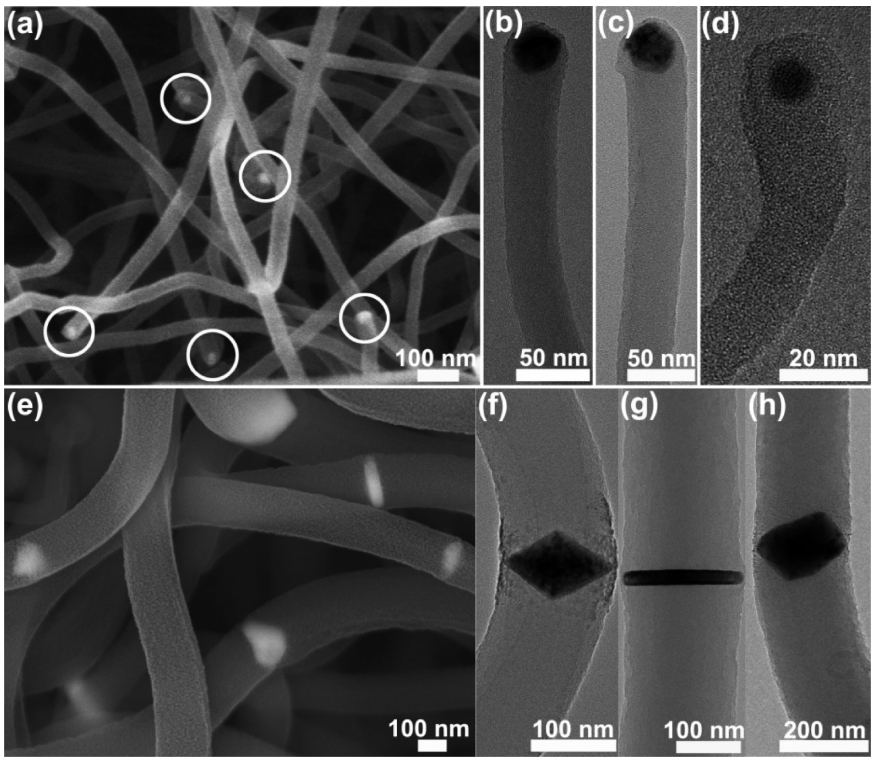

Figure 5. (a) High-magnification SEM image of TNFs obtained by applying 200 ALD cycles of CuO. Typical TEM images of a single TNF with Cu nanoparticles located at one end by applying (b, c) 200 and (d) 100 ALD cycles of CuO. (e) High-magnification SEM image of TKFs obtained by applying 1200 ALD cycles of CuO. (f–h) TEM images of a single TKF with typical faceted Cu nanoparticles located at the middle.

TABLE 1. Systematic Statistics Reflecting the Relationship between the Particle Size of the Catalyst and Morphology of Carbon Products

products	catalyst size (nm)	growth mode	catalyst location	catalyst shape	fiber diameter (nm)
TNF	5–35	straight	single end	spherical	10–40
TNF/CNC	35–50	straight/helical	single end/middle	spherical/polyhedral	40–60
CNC	50–80	helical	middle	polyhedral	60–100
CNC/TKF	80–100	helical/straight	middle	polyhedral	90–120
TKF	100–200	straight	middle	polyhedral	100–250

diameter of 10–40 nm. Figure 5e shows the high-magnification SEM image of TKFs obtained by applying 1200 ALD cycles of CuO. The TKFs are composed of two linear segments with the same length symmetrically grown on two sides of a single catalytic particle. Furthermore, most of these catalyst particles seem to also have a faceted shape, such as octahedron and triangular prism (Figures 5f–h), and the long axis size of catalysts perpendicular to the fiber growth directions is about 80–200 nm. EDS spectra and HRTEM images (Figures S6 and S7) from a single catalyst nanoparticle confirm the feature of face-centered cubic phase of Cu.

From the analyses mentioned above, it can be found that the products have a size-dependent growth morphology. To further probe in detail the growth mechanism of carbon nanostructures, statistics on the particle size of catalysts were obtained by means of TEM observations. As shown in Table 1, we can clearly see the relationship between the morphology of carbon products and the size of catalyst particles. When the particle size is smaller than 35 nm, only TNFs with the single-ended and linear growth mode can be obtained. While the particle sizes are in the range between 50 and 80 nm, high-purity CNCs can be obtained with a mirror-symmetric growth mode and elegant helical structure. Finally, a further increase of particle size to more than 100 nm leads to high-yield TKFs with a linear structure. The extensive investigations by FE-SEM and TEM also show that all the fiber diameters of the TNFs, CNCs, and TKFs increase with the increasing particle size of the catalyst.

To date, various mechanisms have been proposed for the formation of coiled carbon nanostructures. For instance, helically coiled single-walled nanotubes could possibly be due to the regular insertion of pentagon–heptagon pairs at the junctions.[35] Biró *et al.* reinforced further the mechanism and suggested

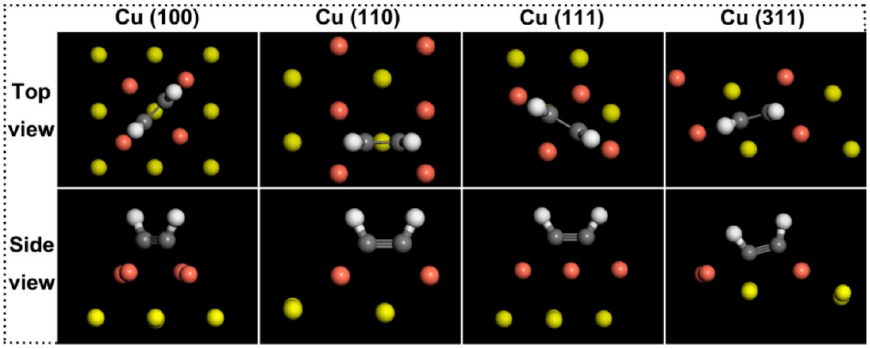

Figure 6. Adsorption sites of acetylene on Cu(100), (110), (111), and (311) surfaces. Cu atoms are denoted by red (the first layer) and yellow (internal layers) balls; C and H atoms are shown in gray and white, respectively.

that the metastable states of nonhexagonal units that cannot anneal out at low growth temperature contribute to the growth of helical carbon nanotubes.[36] Amorphous CNCs can be explained by the "anisotropy of carbon deposition" among the three crystal facets.[37] However, the present nanofibers are entirely different from the carbon nanofibers prepared by carbon deposition of acetylene on Ni, Co, and Fe nanoparticles at high temperature. The FTIR spectrum (Figure S8) reveals that the chemical structure of CNCs consists of both C═C and saturated CH_2 and CH_3 groups. They have a polymer-like structure derived from the adsorption of acetylene on the Cu surface followed by polymerization *via* heterogeneous catalysis.[33] The adsorption behavior of C_2H_2 on different Cu crystal planes was also studied by DFT calculations. We calculated the possible high (221, 311, and 331) and low (100, 110, and 111) index faces for C_2H_2 adsorption (Figure 6 and Table 2). For high-index faces, energetically stable 2-fold hollow (TFH) adsorption was found on the Cu(311) surface, while adsorption of C_2H_2 molecules is unstable on other high-index surfaces such as Cu(221) and (331). For low-index planes it was found that the adsorption of C_2H_2 molecules on Cu(111) are more favorable than on Cu(100) and (110), which is similar to that reported previously.[15,19] In this work, the obtained products exhibit a particle size-dependent morphology determined by the ALD cycle numbers for the initial CuO nanoparticles. On the basis of the observed results and the calculated data, we can basically explicate the formation mechanism of the particle size-dependent morphology.

When a small ALD cycle number (<200 cycles) was applied for CuO, Cu nanoparticles with a small size (<35 nm) were obtained after reduction. It is well known that small-sized nanoparticles tend to adopt a spherical shape with dominantly exposed high-index surfaces.[38,39] The calculated results revealed that only (311) surfaces were found to be energetically stable for C_2H_2 adsorption. However, C_2H_2 is not unstably adsorbed on other high-index surfaces, and the adsorption results in collapse/reconstruction of the corresponding surfaces (Figure S9). Therefore, the small-sized Cu

TABLE 2. Computed Adsorption Energies (E_{ad}) of C_2H_2 on Different Cu Facets

surface	C—C bond length (Å)	C—C—H angle (deg)	adsorption site	E_{ad} (eV)
Cu(311)	1.389	117.61	TFH	1.68
Cu(111)	1.369	121.70	TFH	1.62
Cu(100)	1.372	119.63	TFH	1.34
Cu(110)	1.382	116.61	FFH	1.03

nanoparticles are present with a metastable spherical shape due to the collapse/reconstruction of the surface caused by C_2H_2 adsorption during nanofiber growth. The catalytic isotropy of such metastable spherical Cu nanoparticles is responsible for the single-ended and linear growth of carbon nanofibers, similar to the nanoeffect reported previously.[19]

With increased ALD cycle number of CuO, the resulting Cu nanoparticles can be exposed dominantly with low-index faces including (111), (100), and (110). At the same time, facets tended to form on the particle surface to increase the portion of the low-index planes (particularly, (111) faces) with a high lattice density and low surface energy upon adsorption of C_2H_2,[40] resulting in reconstruction of the Cu nanoparticles in shape. This is the reason that the particles usually have an octahedron or triangular prism shape. It can be seen from Table 2 that the adsorption energies of acetylene on different crystal faces of Cu are 1.62, 1.34, and 1.03 for (111), (100), and (110), respectively. In this case, the remarkably different adsorption energy imposes dramatic growth anisotropy on Cu nanoparticle surfaces for carbon nanofibers, thus leading to the growth of CNCs.

When the size of the Cu nanoparticles is further increased (over 100 nm), the particles undergo difficult deformation, resulting in decreased regularity in shape after reconstruction. Moreover, the fiber diameter will increase accordingly. The large fiber diameter necessitates a larger torsion for the fibers to grow in a helical morphology. Therefore, instead of CNCs, two-directional straight fibers are produced when the Cu particle size is larger than 100 nm even if they have a faceted shape with dominantly exposed low-index surfaces.

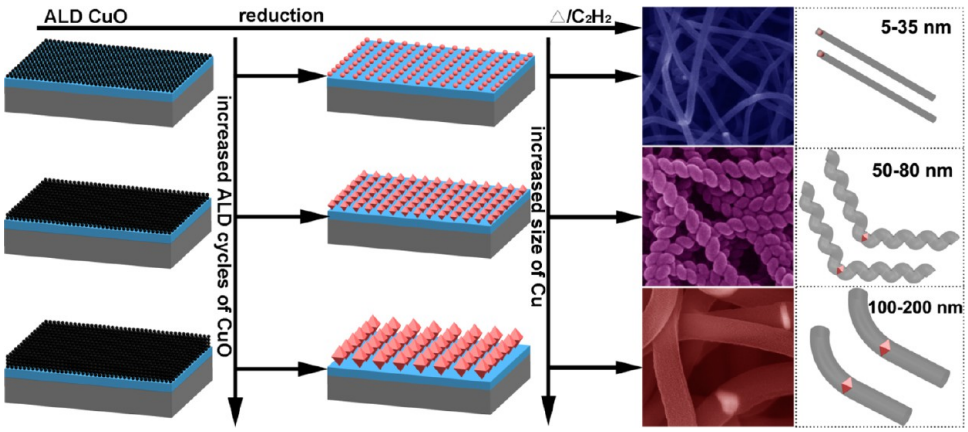

Figure 7. Schematic illustration of the growth pathway of TNFs, CNCs, and TKFs depending on the size of the Cu nanoparticles by controlling the ALD cycle number of CuO.

The HRTEM investigation of Cu particles with different sizes (Figure 3i and j, Figures S6, S7, and S10−12) clearly reveals that the exposed facets play an important role in the resulting morphologies of the carbon nanostructures. A schematic growth process of TNFs, CNCs, and TKFs based on size-independent Cu nanoparticles is shown in Figure 7. Obviously, ALD provides a simple way to prepare catalysts with uniform particle size for the controlled growth of highly pure CNCs.

High-temperature heat treatment of carbon fibers can remove the noncarbon element and enhance their physical properties including electrical conductivity, Young's modulus, thermal expansion coefficient, and strength, which are particularly attractive for potential applications in aeronautics (braking systems) and aerospace (heat shields) and military applications. In this work, we found the elegant spiral morphology can be well preserved after carbonization at 900 °C (Figure S13a and b). The HRTEM image (Figure S13c) shows that the fiber consists of less ordered graphitic layers. Even when the heat treatment temperature was increased to 2800 °C, the products still exhibit a nice helical structure, with almost no change in their diameters (Figure S14a and b). HRTEM investigations (Figure S14c and d) confirm the structure of the sample obtained at 2800 °C is completely different and the carbon layer tends toward the well-organized structure of crystalline graphite. In agreement with a previous paper,[41] the (002) lattice fringe image of the graphitized fiber shows small stacks of nanometer-sized layers. At this temperature, pyrolysis of the fiber gives a carbon with an anisotropic fibrous texture with a preferential orientation perpendicular to the fiber axis at both surfaces and bends. In addition, it should be noticed that such a heat treatment is also helpful for removing catalysts as the pore was produced because of Cu particle evaporation (Figure S14e). Such a significant improvement in the structure of the material is also demonstrated by the Raman spectra (Figure S15) of CNCs after heat treatment at different temperatures. The well-preserved morphology and transformational arrangement of carbon layers under heat treatment may enhance the prospects of CNCs for applications in the fields of mechanics, electronics, and magnetics.

CONCLUSIONS

In summary, we have demonstrated the controllable and reproducible synthesis of nearly 100% pure CNCs with Cu nanoparticles produced by ALD as catalysts. Such CNCs exhibit a symmetric growth mode with uniform fiber diameter, coil diameter, and coil pitch. Through convenient adjustment of ALD cycle numbers of CuO, we investigated the effect of the particle size on the selective growth of CNCs and revealed a legible particle size-dependent growth process: from thin straight fiber to helical fiber to thick straight fiber. A definitional range on the particle size of catalyst for selective CNC growth is proposed based on systematical investigations, which will give guidance to obtain highly pure CNCs in future work and trigger their use in a wide range of fields, including mechanics, electronics, and magnetics. The prominent advantages of ALD offer us the possibility for convenient synthesis of catalytic particles with highly controllable size and size distribution to study particle size-dependent catalytic behavior.

EXPERIMENTAL SECTION

Experimental Procedure. Typically, n-type Si(100) wafers were used as substrates in this study. Prior to the deposition, the Si substrates were initially treated by a cleaning process, which involved washing in acetone, rinsing in deionized water, and blow-drying with nitrogen to remove contaminants. The ALD process was carried out in a hot-wall flow-type ALD reactor. The substrates were first coated with 5 nm of Al_2O_3 by ALD to stabilize the catalyst and avoid the penetration between Cu and Si. The Al_2O_3 film was deposited at 150 °C with trimethylaluminum ($Al(CH_3)_3$) and deionized H_2O as precursors. The growth rate for Al_2O_3 was about 1.0 Å per cycle. The CuO was

deposited by sequential exposure of the substrates to copper bis(2,2,4,6-tetramethyl-3,5-heptanedionate) [$Cu(thd)_2$] and O_3. The deposition temperature was 250 °C, and $Cu(thd)_2$ was kept at 160 °C. Finally, after the ALD process, the substrates were transferred to a tube furnace (a quartz tube, 60 mm in diameter and 1100 mm in length), and then a stream of acetylene was introduced. The growth of CNCs was performed at 260 °C for 20 min at atmospheric pressure. After the apparatus was cooled to room temperature, the as-prepared samples were obtained.

Characterization of the Samples. X-ray photoelectron spectra (XPS) were recorded on an AXIS ULTRA DLD spectrometer (Shimadzu/Kratos) to characterize the surface composition of ALD films with the Al Kα line as the excitation source. The X-ray diffraction (XRD) patterns were collected on a Bruker D8 Advance X-ray diffractometer with Cu Kα radiation (λ = 1.54178 Å) using a 40 kV operation voltage and 40 mA current. The TEM, SAED, and HRTEM images were taken on a JEOL JEM-2100 microscope instrument at an acceleration voltage of 200 kV. The composition of the samples was analyzed by EDS attached to the TEM instrument. The surface morphologies of ALD CuO films were examined by SEM operated at a Hitachi S-4800 with an accelerating voltage of 15 kV. Fourier transform infrared spectroscopy (FTIR) spectra were collected on a Bruker TENSOR27 spectrometer, and the sample was prepressed with KBr into pellets before measurement.

Computational Details. The chemisorption of acetylene on crystal planes of Cu(100), (110), (111), (221), (331), and (311) was studied by density functional theory (DFT)[42] calculations with the generalized gradient approximation (GGA) of Perdew and Wang,[43] as implemented in the DMol^3 package.[44] The surface was treated with the slab model, and the slabs are separated by a 15 Å vacuum thickness. A supercell of 2 × 2 × 5 and fine mesh points were chosen in the simulation.

Conflict of Interest: The authors declare no competing financial interest.

Acknowledgment. This work was financially supported by National Natural Science Foundation of China (21376256, 21173248, 21203229, 51362010), the Hundred Talent Program of the Chinese Academy of Sciences, the Hundred Talent Program of Shanxi Province, and in-house projects of State Key Laboratory of Coal Conversion of China (Y2BWLD1931, Y3BWLE1931).

Supporting Information Available: SEM images of 200, 800, and 1200 ALD cycles of CuO; SEM images of CNCs obtained by using 300 and 450 ALD cycles of CuO; EDS, XRD, and FTIR patterns of CNCs; TEM, EDS, and HRTEM of TNFs and TKFs; atomic arrangement of Cu(211) and (331) surfaces before and after C_2H_2 adsorption; TEM and HRTEM images of carbonized and graphitized CNCs; Raman spectra of carbonized and graphitized CNCs. This material is available free of charge *via* the Internet at http://pubs.acs.org.

REFERENCES AND NOTES

1. Bajpai, V.; Dai, L.; Ohashi, T. Large-Scale Synthesis of Perpendicularly Aligned Helical Carbon Nanotubes. *J. Am. Chem. Soc.* **2004**, *126*, 5070–5071.
2. Amelinckx, S.; Zhang, X.; Bernaerts, D.; Zhang, X.; Ivanov, V.; Nagy, J. B. A Formation Mechanism for Catalytically Grown Helix-Shaped Graphite Nanotubes. *Science* **1994**, *265*, 635–639.
3. Wang, W.; Yang, K.; Gaillard, J.; Bandaru, P. R.; Rao, A. M. Rational Synthesis of Helically Coiled Carbon Nanowires and Nanotubes through the Use of Tin and Indium Catalysts. *Adv. Mater.* **2008**, *20*, 179–182.
4. Akagi, K.; Tamura, R.; Tsukada, M.; Itoh, S.; Ihara, S. Electronic Structure of Helically Coiled Cage of Graphitic Carbon. *Phys. Rev. Lett.* **1995**, *74*, 2307.
5. Tang, N.; Kuo, W.; Jeng, C.; Wang, L.; Lin, K.; Du, Y. Coil-in-Coil Carbon Nanocoils: 11 Gram-Scale Synthesis, Single Nanocoil Electrical Properties, and Electrical Contact Improvement. *ACS Nano* **2010**, *4*, 781–788.
6. Volodin, A.; Buntinx, D.; Ahlskog, M.; Fonseca, A.; Nagy, J. B.; Van Haesendonck, C. Coiled Carbon Nanotubes as Self-Sensing Mechanical Resonators. *Nano Lett.* **2004**, *4*, 1775–1779.
7. Chen, X.; Zhang, S.; Dikin, D. A.; Ding, W.; Ruoff, R. S.; Pan, L.; Nakayama, Y. Mechanics of a Carbon Nanocoil. *Nano Lett.* **2003**, *3*, 1299–1304.
8. Wang, G.; Gao, Z.; Tang, S.; Chen, C.; Duan, F.; Zhao, S.; Lin, S.; Feng, Y.; Zhou, L.; Qin, Y. Microwave Absorption Properties of Carbon Nanocoils Coated with Highly Controlled Magnetic Materials by Atomic Layer Deposition. *ACS Nano* **2012**, *6*, 11009–11017.
9. Tang, N.; Zhong, W.; Au, C.; Yang, Y.; Han, M.; Lin, K.; Du, Y. Synthesis, Microwave Electromagnetic, and Microwave Absorption Properties of Twin Carbon Nanocoils. *J. Phys. Chem. C* **2008**, *112*, 19316–19323.
10. Liu, W.; Lin, H.; Chen, Y.; Lee, C.; Chiu, H. Growth of Carbon Nanocoils from K and Ag Cooperative Bicatalyst Assisted Thermal Decomposition of Acetylene. *ACS Nano* **2010**, *4*, 4149–4157.
11. Tsou, T.; Lee, C.; Chiu, H. K and Au Bicatalyst Assisted Growth of Carbon Nanocoils from Acetylene: Effect of Deposition Parameters on Field Emission Properties. *ACS Appl. Mater. Interfaces* **2012**, *4*, 6505–6511.
12. Umari, M.; Varadan, V.; Varadan, V. Rotation and Dichroism Associated with Microwave Propagation in Chiral Composite Samples. *Radio Sci.* **1991**, *26*, 1327–1334.
13. Sharma, R.; Balakrishnan, N. Scattering of Electromagnetic Waves from Arbitrary Shaped Bodies Coated with a Chiral Material. *Smart Mater. Struct.* **1998**, *7*, 851–866.
14. Pan, L.; Konishi, Y.; Tanaka, H.; Suekane, O.; Nosaka, T.; Nakayama, Y. Effect of Morphology on Field Emission Properties of Carbon Nanocoils and Carbon Nanotubes. *Jpn. J. Appl. Phys.* **2005**, *44*, 1652–1654.
15. Jian, X.; Jiang, M.; Zhou, Z.; Yang, M.; Lu, J.; Hu, S.; Wang, Y.; Hui, D. Preparation of High Purity Helical Carbon Nanofibers by the Catalytic Decomposition of Acetylene and Their Growth Mechanism. *Carbon* **2010**, *48*, 4535–4541.
16. Zhao, M.; Zhang, Q.; Zhang, W.; Huang, J.; Zhang, Y.; Su, D.; Wei, F. Embedded High Density Metal Nanoparticles with Extraordinary Thermal Stability Derived from Guest-Host Mediated Layered Double Hydroxides. *J. Am. Chem. Soc.* **2010**, *132*, 14739–14741.
17. Zhang, Q.; Zhao, M.; Tang, D.; Li, F.; Huang, J.; Liu, B.; Zhu, W.; Zhang, Y.; Wei, F. Carbon-Nanotube-Array Double Helices. *Angew. Chem., Int. Ed.* **2010**, *122*, 3642–3645.
18. Qin, Y.; Zhang, Z.; Cui, Z. Helical Carbon Nanofibers Prepared by Pyrolysis of Acetylene with a Catalyst Derived from the Decomposition of Copper Tartrate. *Carbon* **2003**, *41*, 3072–3074.
19. Jian, X.; Jiang, M.; Zhou, Z.; Zeng, Q.; Lu, J.; Wang, D.; Zhu, J.; Gou, J.; Wang, Y.; Hui, D. Gas-Induced Formation of Cu Nanoparticle as Catalyst for High-Purity Straight and Helical Carbon Nanofibers. *ACS Nano* **2012**, *6*, 8611–8619.
20. Tang, N.; Wen, J.; Zhang, Y.; Liu, F.; Lin, K.; Du, Y. Helical Carbon Nanotubes: Catalytic Particle Size-Dependent Growth and Magnetic Properties. *ACS Nano* **2010**, *4*, 241–250.
21. Xia, J.; Jiang, X.; Jia, C. The Size Effect of Catalyst on the Growth of Helical Carbon Nanofibers. *Appl. Phys. Lett.* **2009**, *95*, 223110.
22. Okazaki, N.; Hosokawa, S.; Goto, T.; Nakayama, Y. Synthesis of Carbon Tubule Nanocoils Using Fe-In-Sn-O Fine Particles as Catalysts. *J. Phys. Chem. B* **2005**, *109*, 17366–17371.
23. Li, D.; Pan, L.; Qian, J.; Liu, D. Highly Efficient Synthesis of Carbon Nanocoils by Catalyst Particles Prepared by a Sol-Gel Method. *Carbon* **2010**, *48*, 170–175.
24. Hirahara, K.; Nakayama, Y. The Effect of a Tin Oxide Buffer Layer for the High Yield Synthesis of Carbon Nanocoils. *Carbon* **2013**, *56*, 264–270.
25. George, S. M. Atomic Layer Deposition: An Overview. *Chem. Rev.* **2009**, *110*, 111–131.
26. Knez, M.; Nielsch, K.; Niinistö, L. Synthesis and Surface Engineering of Complex Nanostructures by Atomic Layer Deposition. *Adv. Mater.* **2007**, *19*, 3425–3438.

27. Marichy, C.; Bechelany, M.; Pinna, N. Atomic Layer Deposition of Nanostructured Materials for Energy and Environmental Applications. *Adv. Mater.* **2012**, *24*, 1017–1032.
28. Lu, J.; Elam, J. W.; Stair, P. C. Synthesis and Stabilization of Supported Metal Catalysts by Atomic Layer Deposition. *Acc. Chem. Res.* **2013**, *46*, 1806–1815.
29. Christensen, S. T.; Feng, H.; Libera, J. L.; Guo, N.; Miller, J. T.; Stair, P. C.; Elam, J. W. Supported Ru-Pt Bimetallic Nanoparticle Catalysts Prepared by Atomic Layer Deposition. *Nano Lett.* **2010**, *10*, 3047–3051.
30. King, J. S.; Wittstock, A.; Biener, J.; Kucheyev, S. O.; Wang, Y. M.; Baumann, T. F.; Giri, S. K.; Hamza, A. V.; Baeumer, M.; Bent, S. F. Ultralow Loading Pt Nanocatalysts Prepared by Atomic Layer Deposition on Carbon Aerogels. *Nano Lett.* **2008**, *8*, 2405–2409.
31. Feng, H.; Elam, J. W.; Libera, J. A.; Setthapun, W.; Stair, P. C. Palladium Catalysts Synthesized by Atomic Layer Deposition for Methanol Decomposition. *Chem. Mater.* **2010**, *22*, 3133–3142.
32. Galtayries, A.; Bonnelle, J. P. XPS and ISS Studies on the Interaction of H_2S with Polycrystalline Cu, Cu_2O and CuO Surfaces. *Surf. Interface Anal.* **1995**, *23*, 171–179.
33. Qin, Y.; Jiang, X.; Cui, Z. Low-Temperature Synthesis of Amorphous Carbon Nanocoils *via* Acetylene Coupling on Copper Nanocrystal Surfaces at 468 K: A Reaction Mechanism Analysis. *J. Phys. Chem. B* **2005**, *109*, 21749–21754.
34. Dong, L.; Yu, L.; Cui, Z.; Dong, H.; Ercius, P.; Song, C.; Duden, T. Direct Imaging of Copper Catalyst Migration inside Helical Carbon Nanofibers. *Nanotechnology* **2012**, *23*, 035702.
35. Dunlap, B. I. Connecting Carbon Tubules. *Phys. Rev. B* **1992**, *46*, 1933–1936.
36. Biró, L. P.; Márk, G. I.; Koós, A. A.; Nagy, J. B.; Lambin, P. Coiled Carbon Nanotube Structures with Supraunitary Nonhexagonal to Hexagonal Ring Ratio. *Phys. Rev. B* **2002**, *66*, 165405.
37. Motojima, S.; Chen, Q. Three-Dimensional Growth Mechanism of Cosmo-Mimetic Carbon Microcoils Obtained by Chemical Vapor Deposition. *J. Appl. Phys.* **1999**, *85*, 3919–3921.
38. Yang, M.; Jackson, K. A.; Koehler, C.; Frauenheim, T.; Jellinek, J. Structure and Shape Variations in Intermediate-Size Copper Clusters. *J. Chem. Phys.* **2006**, *124*, 024308.
39. Jiang, M.; Zeng, Q.; Zhang, T.; Yang, M.; Jackson, K. A. Icosahedral to Double-Icosahedral Shape Transition of Copper Clusters. *J. Chem. Phys.* **2012**, *136*, 104501.
40. Hansen, P. L.; Wagner, J. B.; Helveg, S.; Rostrup-Nielsen, J. R.; Clausen, B. S.; Topsøe, H. Atom-Resolved Imaging of Dynamic Shape Changes in Supported Copper Nanocrystals. *Science* **2002**, *295*, 2053–2055.
41. Vázquez-Santos, M. B.; Martínez-Alonso, A.; Tascón, J.; Rouzaud, J.; Geissler, E.; László, K. Complementary X-Ray Scattering and High Resolution Imaging of Nanostructure Development in Thermally Treated PBO Fibers. *Carbon* **2011**, *49*, 2960–2970.
42. Hohenberg, P.; Kohn, W. Inhomogeneous Electron Gas. *Phys. Rev.* **1964**, *136*, B864–B871.
43. Perdew, J. P.; Wang, Y. Accurate and Simple Analytic Representation of the Electron-Gas Correlation Energy. *Phys. Rev. B* **1992**, *45*, 13244–13249.
44. Delley, B. From Molecules to Solids with the $DMol^3$ Approach. *J. Chem. Phys.* **2000**, *113*, 7756–7764.